

The Changing Sensitivity of Wintertime Particulate Nitrate to Precursor Emissions Diagnosed via GEOS-Chem and Satellite Observations of Ammonia and Nitrogen Dioxide over the Midwestern United States

5 Toan Vo¹, Amy E. Christiansen^{1*}

¹ Division of Energy, Matter & Systems, University of Missouri – Kansas City, MO, 64110

*Correspondence to: Amy E. Christiansen (achristiansen@umkc.edu)

Abstract. Particulate nitrate (PN) is a critical component of fine particulate matter (PM_{2.5}). During wintertime, the contribution of PN to PM_{2.5} over the Midwestern United States (MWUS), an agriculturally intensive region, has increased over the past decade and now contributes up to 40% of the particle mass. PN formation is controlled by nitrogen oxides (NO_x = NO + NO₂), ammonia (NH₃), and volatile organic compounds (VOCs). To best control wintertime PM_{2.5} burden, it is critical to determine PN formation sensitivity to precursor gases, but this is not well constrained. Prior efforts to diagnose PN sensitivity have been limited on both spatial and temporal scales. Satellite tropospheric column NH₃/NO₂ ratios cover large areas and long timeframes, and they have been shown to be effective in diagnosing PN sensitivity over East Asia, Europe, and the Eastern United States. Here, we expand this approach to quantify spatially and temporally resolved multidecadal wintertime PN formation sensitivity to NH₃, NO_x, and VOCs in the MWUS from 2007 to 2023 via satellite observations and GEOS-Chem sensitivity simulations. More than half of the total diagnosed pixels are classified as NO_x-sensitive in 2007, and this increases to 89.0% by 2023. VOCs do not control MWUS PN formation. The shift in PN formation sensitivity is explained by relatively flat trends in satellite NO₂ column densities ($0.48 \pm 0.60\% \text{ yr}^{-1}$) in combination with increases in satellite NH₃ column densities ($1.3 \pm 0.3\% \text{ yr}^{-1}$). Our work indicates that targeting NO_x emissions is chemically effective for reducing wintertime PN and PM_{2.5} burden.

1. Introduction

PM_{2.5}, particulate matter with an aerodynamic diameter of 2.5 μm or less, is the largest environmental health risk factor in the United States (Di et al., 2017; Pokharel et al., 2023; Shi et al., 2022; Tessum et al., 2019; Wu et al., 2018). PM_{2.5} is formed via acid-base reactions between the acidic precursor species, nitrogen oxides (NO_x = NO + NO₂) and sulfur dioxide (SO₂), and the basic gas ammonia (NH₃) to form ammonium sulfate and ammonium nitrate. Regulations on SO₂ and NO_x emissions via the Clean Air Act have led to notable decreases in the PM_{2.5} burden across the United States over the past few decades, primarily through the reduction in particulate nitrate (PN) and particulate sulfate (PS) (Hand et al., 2012). PS, which has historically dominated the inorganic fraction of PM_{2.5}, has decreased more quickly than PN, increasing the relative contribution of PN to total PM_{2.5} mass. PN concentrations are highest during wintertime because the gas-to-particle partitioning

of PN is favored at low temperatures (Pitchford et al., 2009). During wintertime over the Midwestern United States (MWUS), a highly agricultural region, the PN/PS ratio has increased, as PS has decreased at a faster rate compared to PN over the past decade (Figure S1). The increase in relative PN abundance may also be influenced by increases in the atmospheric lifetime of total nitrate during wintertime (Zhai et al., 2021). Over the MWUS, wintertime PN now comprises up to 40% of the total PM_{2.5} mass on average.

PN is highly hygroscopic, which affects particle properties and enhances the reflectivity of particles (Wang et al., 2018; Wu et al., 2019). PN has been found to drive pollution events over certain regions of the US (Franchin et al., 2018; Womack et al., 2019) and the globe (Qin et al., 2024; Xu et al., 2019). PN has also become the controlling factor behind particle water uptake in some regions, impacting particle chemical processes and visibility (Christiansen et al., 2020; Jefferson et al., 2017). Recent studies have shown that the products from PN photolysis may influence the formation of tropospheric O₃ and thus atmospheric oxidation capacity (Cao et al., 2022; Gen et al., 2022; Sarwar et al., 2024). It is critical to accurately understand PN properties and formation to better understand PN impacts and create effective policy that controls PM_{2.5} burden.

NO_x, NH₃, and volatile organic compounds (VOCs) are critical to the formation of PN (Wang et al., 2023a). During the daytime, NO₂ is oxidized to HNO₃ via reaction with hydroxyl radical ([•]OH). HNO₃ then reacts with NH₃ to form ammonium nitrate, which partitions into the particle phase. During nighttime, PN is formed via the heterogenous hydrolysis of N₂O₅, which is formed from the oxidation of NO₂ with ozone (O₃). In these mechanisms, the availability of [•]OH and O₃ are highly dependent on VOC abundance. Thus, PN formation is sensitive to the precursor gases NO_x, NH₃, and VOCs, and its formation is controlled by whichever precursor gas is the limiting reagent. Competing mechanisms with organic molecules also contribute to total PN, but the exact mechanisms and processes behind organo-nitrate formation are not well constrained, and inorganic nitrate is most prominent in particles (Romer Present et al., 2020; Wang et al., 2023a).

Precursor gas emissions have changed drastically over the past few decades, potentially altering PN formation sensitivity and its relative contribution to total PM_{2.5} mass. Urban NO_x emissions dominated by anthropogenic sources have decreased by 40% from 2005 to 2018 across the US (Jiang et al., 2022). Over rural areas, total surface NO₂ trends decreased strongly until 2010, after which they flattened. The decreasing prevalence of urban NO_x emissions have caused rural total NO_x trends to be influenced more strongly by relatively constant background emissions (e.g., lightning, soil, etc.), and NO_x trends over rural areas post-2010 are typically insignificant (Christiansen et al., 2024; Jiang et al., 2022; Silvern et al., 2019). Satellite NO₂ column densities show similar flattening trends after 2010, which is attributed to the increasingly strong relative influence of free tropospheric NO₂ in satellite column trends (Dang et al., 2023a; Fioletov et al., 2022; He et al., 2022; Jiang et al., 2018; Tong et al., 2015; Wang et al., 2021).

In contrast, NH₃ is not regulated as a criterion pollutant, although there exist some regulations on agricultural NH₃ practices, which target livestock emissions (United States Environmental Protection Agency, 2014). Recently, satellite NH₃ column densities have increased strongly over the US ($2.40 \pm 0.45\% \text{ yr}^{-1}$ from 2002 to 2018), which matches increases in surface NH₃ concentrations (Van Damme et al., 2021; Wang et al., 2023b, Yu et al., 2018). The increase in NH₃ concentrations over the agricultural Central United States is disproportionately higher than over the US as a whole, ranging from 1–7% yr⁻¹ (Yu et al.,

65 2018). This increase can be explained by increases in emissions from both agriculture (Vo and Christiansen, 2024; Yang et al., 2023) and vehicles (Fenn et al., 2018; Sun et al., 2017; Walters et al., 2022), as well as decreases in NO₂ and SO₂ emissions that increase unreacted NH₃ abundance (Warner et al., 2017).

Anthropogenic VOC emissions are low during winter, but they have continuously decreased over time. Urban VOC emissions over the United States have decreased by -36.4% from 2000 to 2019, which is attributable to decreases in transportation and industrial solvent emissions (Xiong et al., 2024). Emissions of isoprene, a biogenic VOC, conversely showed an increase of 0.14% yr⁻¹ from 2000 to 2020 in US, which is primarily influenced by meteorological factors and changes in vegetation coverage (Wang et al., 2024).

To most effectively reduce PM_{2.5} burden, it is critical to understand how these large changes in precursor gas emissions have influenced PN formation sensitivity over time. Over past decades, controlling NH₃ emissions has been suggested to be most effective in reducing wintertime PM_{2.5} burden over agricultural regions, but more recent analyses suggest that NO_x controls may now be more effective, although at a higher cost and more technologically complex approach than NH₃ controls (Guo et al., 2024; Holt et al., 2015; Pan et al., 2024; Paulot et al., 2014; Pinder et al., 2007; Wiegand et al., 2022). Therefore, the most effective strategy to control PN and PM_{2.5} in agriculturally impacted areas, such as the MWUS regions, remains an open question. Few prior studies have attempted to diagnose PN and PM_{2.5} sensitivity to precursor gases in the MWUS. Holt et al. (2015) diagnosed the wintertime inorganic PM_{2.5} sensitivity over the US to NO_x, NH₃, and SO₂ emissions between 2005 and 2012 using only GEOS-Chem simulations and found that NO_x sensitivity increased over time (Holt et al., 2015). Dang et al. (2024) conducted a PN formation sensitivity diagnosis over the US across all seasons in 2017, but this focused mostly on the Eastern US and covered very little of agricultural MWUS (Dang et al., 2024). Neither of these studies captured the long-term (multidecadal) dynamics of wintertime PN formation sensitivity over highly agricultural areas.

Determining PN formation sensitivity has traditionally proven challenging. Methods used in previous studies are subject to large uncertainties, especially in the measurement of HNO₃ (Franchin et al., 2018; Petetin et al., 2016), are computationally intensive (Paulot et al., 2016; Shimadera et al., 2014; Zhai et al., 2021), and typically have only been applied to short timeframes (Nenes et al., 2020; Wen et al., 2018; Zhai et al., 2023). Recently, Dang et al. (2023) introduced an innovative approach to overcome these limitations and diagnose PN sensitivity using satellite tropospheric column NH₃/NO₂ ratios and chemical transport models without the need for HNO₃ measurements or exceedingly computationally intensive calculations (Dang et al., 2023b). Importantly, this method can quickly diagnose PN sensitivity to precursor gases across a broad region and a longer timeframe due to the large spatial and temporal coverage of satellite observations. This approach has been applied on short timeframes over East Asia, Europe, and the Eastern United States across all seasons with high accuracy when compared to previous studies (Dang et al., 2024). Here, we will expand this methodology over the MWUS to track multidecadal changes in wintertime PN formation sensitivity.

In this work, we evaluate changes in wintertime PN formation sensitivity by quantifying the changes in the sensitivity regime of wintertime PN to NH₃, NO_x, and VOCs over the MWUS from 2007 to 2023 via satellite observations of NO₂ and NH₃ column density and model sensitivity simulations. We also explore whether controlling NO_x emissions or controlling NH₃

emissions is the best PN and PM_{2.5} mitigation strategy over the MWUS during winter. These methods can be expanded in the
100 future to investigate PN formation sensitivity in other seasons, as both NO₂ and NH₃ exhibit strong seasonality.

2. Methodology:

2.1. Satellite observations:

2.1.1. General information:

NO₂ column density was obtained from the Ozone Monitoring Instrument (OMI) using version 4.0 of the NASA
105 OMI/Aura NO₂ Level 2 product (https://disc.gsfc.nasa.gov/datasets/OMNO2_003/summary). OMI is operated onboard the sun-synchronous NASA Earth Observing System (EOS) Aura satellite (Krotkov et al., 2019). NO₂ is detected at visible wavelengths (402–465 nm), and the measurements are in swaths of 2,600 km width at 13:45 ± 0:15 local solar time (Lamsal et al., 2021).

NH₃ column density was obtained from the Infrared Atmospheric Sounding Interferometer (IASI) onboard the Metop-A
110 and Metop-B sun-synchronous satellites (Clarisse et al., 2018a, 2018b) (<https://iasi.aeris-data.fr/catalog/?currentSelection=871d9366-22d7-4d8d-997e-02e7721f7e94#masthead> for Metop-A; <https://iasi.aeris-data.fr/catalog/?currentSelection=44a739bf-8b68-4b64-b594-d7bb3fbc40bf#masthead> for Metop-B). Here, we use the reanalyzed daily IASI/Metop-A (2007–2020) and IASI/Metop-B (2021–2023) dataset (ANNI-NH3-v4R). This satellite provides measurements twice daily in the morning (9:30 local solar time) and the evening (21:30 local solar time) (Van Damme et al., 2014). In this study, we use only morning overpass measurements to minimize time separation from OMI (13:45 ± 0:15
115 local solar time). IASI captures backscattered infrared radiation (~645–2760 cm⁻¹) of atmospheric trace gases directly perpendicular to Earth’s surface with a 12-km circular footprint (Clerbaux et al., 2009; Van Damme et al., 2017).

2.1.2. Analyzing satellite observations:

The methodology of this study is summarized in Figure S2. We obtained NO₂ and NH₃ column density from winter 2007
120 to winter 2023 over the MWUS (36° to 49° latitude and –104° to –87° longitude) from OMI and IASI. We used measurements from November, December, January, and February to represent winter to ensure >60% coverage over the MWUS both spatially and temporally due to the limited satellite sensitivity. For NO₂ columns, we filtered out any pixels with solar zenith angle > 85°, cloud fraction > 0.3, terrain reflectivity > 0.3, NO₂ column density < 0, and any observations impacted by the row anomaly, which arose from problems with radiance measurements (Dang et al., 2023b). For NH₃ column density, we then
125 removed any pixels with cloud fraction > 0.1, NH₃ column density < 0, and pixels with limited sensitivity to NH₃ using the post retrieval quality flag (Dang et al., 2023b).

Next, both NO₂ and NH₃ data sets were averaged seasonally to a 0.5° x 0.625° resolution (latitude x longitude) to spatially match the GEOS-Chem simulation pixels (see Section 3), and we removed any grid cells with < 20 successful retrievals to

further reduce noise. We computed the median NO₂ and NH₃ column density for each pixel for each winter to visualize the distribution of precursor gases over MWUS from 2007 to 2023.

To reduce potential errors arising from differences in the assumed vertical profiles between OMI and GEOS-Chem, a correction factor was calculated to adjust air mass factors (AMFs). Differences in underlying vertical profile assumptions can lead to inconsistencies between the model and satellite observations. We replaced the *a priori* profile used in the OMI retrieval to match that of GEOS-Chem to minimize those errors (Visser et al., 2019). For NO₂ column density, we applied the method described by Lamsal et al. (2010), Boersma et al. (2016), and Visser et al. (2019) to derive a correction factor, which we applied to the AMF in OMI for each aggregated grid cell (Equation 1) (Boersma et al., 2016; Lamsal et al., 2010; Visser et al., 2019).

$$AMF_{GC} = AMF_{OMI} \times \frac{\sum_{l=1}^L A_{trop} x_{l,GC}}{\sum_{l=1}^L x_{l,GC}} \quad (1)$$

In (1), AMF_{OMI} is the air mass factor from OMI, A_{trop} is the averaging kernel, and x_{l,GC} is NO₂ column density obtained from GEOS-Chem in molecules cm⁻² (Boersma et al., 2016; Lamsal et al., 2010; Visser et al., 2019). The averaging kernel is obtained by taking the ratios of scattering weight and AMF_{OMI} at each level (Boersma et al., 2016; Palmer et al., 2001). Then, the newly calculated AMFs (AMF_{GC}) were used to correct the NO₂ column density (NO_{2,OMI}) from OMI (Equation 2). In (2), NO_{2,new} is the corrected OMI NO₂ column, with the underlying *a priori* profile replaced by the profile in GEOS-Chem.

$$NO_{2,new} = NO_{2,OMI} \times \frac{AMF_{GC}}{AMF_{OMI}} \quad (2)$$

Note that correction of satellite column densities by replacing *a priori* vertical profiles with those from GEOS-Chem only applies to NO₂ since there is not enough information from IASI to correct satellite NH₃ column densities. We then calculated the winter average of satellite NO₂ and NH₃ from the median of each grid cell over the MWUS for each year from 2007 to 2023. We then computed the wintertime NH₃/NO₂ ratios across the MWUS by overlaying spatial and temporal 0.5° x 0.625° composites of NH₃ and NO₂ column density.

2.2. GEOS-Chem simulations:

Table 1: Description of GEOS-Chem simulations

Model	GEOS-Chem version 14.4.2
Horizontal resolution (latitude x longitude)	Nested 0.5° x 0.625° resolution with the boundary conditions from a global 4° x 5° resolution simulations ^a
Chemistry	14.4.2 ^b
Meteorology	Modern-Era Retrospective analysis for Research and Applications, version 2 (MERRA-2) ^c

Anthropogenic emissions	Community Emissions Data System (CEDS) and National Emissions Inventory 2016 (NEI 2016) ^d
Biomass burning emissions	Quick Fire Emissions Dataset, version 2 (QFED2) ^e

150 (a) Y.X. Wang et al., 2004; (b) DOI: 10.5281/zenodo.12807579; (c) Gelaro et al., 2017; (d) Hoesly et al., 2018; (e) Koster et al., 2018.

We used the 3D chemical transport model GEOS-Chem to examine the sensitivity of PN formation to NO_x, NH₃, and VOCs. The simulation parameters are summarized in Table 1. In this study, we used GEOS-Chem version 14.4.2, and all the simulations were performed at the nested 0.5° x 0.625° horizontal resolution with boundary conditions from a global 4° x 5° resolution simulation (DOI: 10.5281/zenodo.12807579) (Wang et al., 2004). Next, we assumed that January could represent the entire winter season to reduce computational burden (Dang et al., 2023b). Although GEOS-Chem underestimates observed PN mass concentrations, trends in wintertime PN simulated by GEOS-Chem and observations from the IMPROVE and CSN networks agree well ($R^2 > 0.6$ between GEOS-Chem and ground monitoring networks) (Figure S3). We will evaluate the performance of GEOS-Chem furthermore in Section 2.5.

160 All sensitivity simulations were conducted using 72 vertical pressure levels from 2007 to 2022. GEOS-Chem includes detailed HO_x-NO_x-VOC-O₃-BrO_x-aerosol tropospheric chemistry with over 200 species. We used the reanalysis product Modern-Era Retrospective analysis for Research and Applications, Version 2 (MERRA-2), developed by the NASA Global Modeling and Assimilation Office (GMAO), for meteorological inputs (Gelaro et al., 2017). Emissions were computed by the Harvard-NASA Emissions Component (HEMCO) (Keller et al., 2014). All global anthropogenic emissions were provided by the Community Emissions Data System inventory (Hoesly et al., 2018). Until winter 2018, these emissions were overwritten over the CONUS by the National Emissions Inventory 2016 (NEI 2016) at 0.1° x 0.1° resolution, which was created by NEI Collaborative for air quality modeling over the United States (National Emissions Inventory Collaborative, 2019). Since NEI emissions in the model were only available through January 2019, we used the CEDS inventory at the 0.5° x 0.5° resolution after to simulate anthropogenic emissions over the CONUS (Hoesly et al., 2018). Despite some differences in estimates of emissions magnitudes, which mainly arise from differences in horizontal resolution and the methods used in estimating agricultural emissions, the CEDS and NEI2016 inventories show similar trends (Figures S4), and both predict the same wintertime PN sensitivity at various time slices and locations from 2007 to 2019 (see Section 3.1 and Figure S5), suggesting the sensitivity findings are continuous regardless of inventory (Hoesly et al., 2018; Inventory Collaborative 2016v1 Emissions Modelling Platform).

175 Aircraft emissions were taken from the Aviation Emissions Inventory Code 2019 (AEIC 2019), which covered up to 2019 (Simone et al., 2013). Emissions after 2019 were kept constant at 2019 values. Offline soil NO_x emissions were used, which were provided by Hudman et al. (2012), and offline biogenic VOC emissions were provided by the Model of Emissions of Gases and Aerosols from Nature version 2.1 (MEGAN) as implemented by Hu et al. (2015) from 2007 to 2020 (Guenther et al., 2012; Hu et al., 2015; Hudman et al., 2012). Similar to aircraft emissions, emissions after 2020 for soil NO_x and biogenic VOC emissions were kept constant at 2020 values. Biomass burning emissions were provided by the Quick Fire Emissions

Dataset, version 2 (QFED2) (Koster et al., 2015). Thermodynamic PN formation was calculated with ISORROPIA-II (Fountoukis and Nenes, 2007). We used the Luo et al. (2020) wet deposition scheme to improve the accuracy of modelled PN (Luo et al., 2020). The PN photolysis scheme is described by Shah et al. (2023) (Shah et al., 2023).

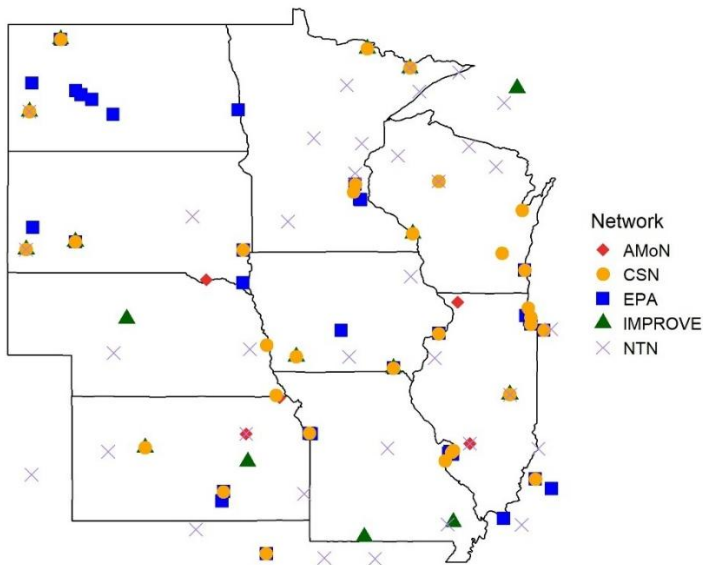
185 Sensitivity simulations used to quantify formation regime cutoffs are summarized in Table 2. The standard simulation (“Base”) was conducted from 2007 to 2022, where no modifications were applied to any emissions. The sensitivity of PN formation to the precursor gases NO_x, NH₃, and VOCs was evaluated with 3 simulations: (1) “Reduced-NO_x”, where NO_x emissions were decreased by 20%; (2) “Reduced-NH₃”, where NH₃ emissions were decreased by 20%; and (3) “Reduced-VOC”, where VOC emissions were decreased by 20%. The total quantities (in Tg) for NO_x, NH₃, and VOC emissions for each sensitivity simulation from 2007 to 2022 are shown in Figure S6. In each sensitivity simulation, the decrease of the precursor
190 gas applied to all emissions sources (natural and anthropogenic). Each sensitivity simulation was run with a full-year spin up for boundary conditions (4° x 5°) followed by one-week spin up for nested simulations (0.5° x 0.625°). Production runs were performed for January of each year. These sensitivity simulations allowed us to examine the influence of each precursor gas on wintertime PN formation, how that sensitivity changed over time, and quantify cutoffs for PN formation regime determination.

195 **Table 2: Description of all sensitivity simulations using GEOS-Chem 14.4.2**

Simulations	NO _x emissions	NH ₃ emissions	VOC emissions
Base	Base	Base	Base
Reduced-NO _x	-20%	Base	Base
Reduced-NH ₃	Base	-20%	Base
Reduced-VOC	Base	Base	-20%

2.3. Ground monitoring observations:

Sites Location for Ground Monitoring Networks



200 Figure 1: Site locations for Ammonia Monitoring Network (AMoN), Chemical Speciation Network (CSN), US Environmental Protection Agency (EPA), Interagency Monitoring of PROtected Visual Environments (IMPROVE), and National Trends Network (NTN) ground monitoring networks. Note that some sites are part of multiple networks.

Table 3: Description of ground monitoring networks.

Name	Retrievals	Number of Sites	Descriptions	Citations
United States Environmental Protection Agency (US EPA) (https://aqs.epa.gov/aqsweb/air_data/download_files.html#Daily)	Surface NO ₂ concentrations	33	24-hour average daily surface NO ₂ concentrations using chemiluminescent detectors, primarily over urban areas.	Demerjian, 2000; United States Environmental Protection Agency. (US EPA; Demerjian, 2000)
National Trends Network (NTN) (https://nadp.slh.wisc.edu/networks/national-trends-network/)	Nitrate wet deposition (NWD)	35	Bi-weekly samples via an automated wet precipitation collector and a rain gauge, mainly located over rural areas.	Lamb and Bowersox, 2000; National Trends Network. (NTN; Lamb and Bowersox, 2000)

Ammonia Monitoring Network (AMoN) (https://nadp.slh.wisc.edu/networks/ammonia-monitoring-network/)	Surface NH ₃ concentrations	9	NH ₃ concentrations using Radiello-brand diffusive samplers located mainly over rural areas.	Puchalski et al., 2015; Ammonia Monitoring Network. (AMoN; Puchalski et al., 2015)
Interagency Monitoring of PROtected Visual Environments (IMRPOVE) (https://views.cira.colostate.edu/fed/QueryWizard/)	PM _{2.5} mass concentrations and chemical speciation (PN, NH ₄ ⁺ , PS, and total organic carbon (OC))	16	24-hour integrated PM _{2.5} and chemical speciation mass concentrations every 3 days over rural areas.	Malm et al., 1994; Solomon et al., 2014; Interagency Monitoring of PROtected Visual Environments. (IMPROVE; Malm et al., 1994; Solomon et al., 2014)
Chemical Speciation Network (CSN) (https://aqs.epa.gov/aqsweb/air_data/download_files.html#Daily)	PM _{2.5} mass concentrations and chemical speciation (PN, NH ₄ ⁺ , PS, and total organic carbon (OC))	32	24-hour integrated PM _{2.5} and chemical speciation mass concentrations every 3 days over urban areas.	Solomon et al., 2014; United States Environmental Protection Agency. (US EPA; Solomon et al., 2014)

205 The descriptions of all ground monitoring observations and the locations of each site are summarized in Figure 1 and Table 3. We define winter in this analysis to be November, December, January, and February to match satellite retrievals. In addition, we analyze trends in gas concentrations, wet deposition, and particle speciation and compare them to satellite NO₂ column densities, NH₃ column densities, and model simulations to place results into context. We assume NWD and surface NH₃ concentrations trends are representative of the entire MWUS. While this introduces uncertainty, the agreement of trends
210 between satellite and ground observations is excellent. This will be further discussed in Section 3.

2.4. PN formation sensitivity diagnostic methods:

We calculated the local PN sensitivity to each precursor gas, S_i , for individual $0.5^\circ \times 0.625^\circ$ grid cells from GEOS-Chem using Equation 3. Here, we calculated the ratio of the changes in monthly PN concentrations to changes in emissions of species i , E_i between the sensitivity and Base simulations. In Equation 3, i is NO_x, NH₃, or VOCs (Dang et al., 2023b).

$$S_i = \frac{\Delta \log(PN)}{\Delta \log(E_i)} \quad (3)$$

215 We then chose all the pixels with sensitivity ratios of $0.95 \leq S_i/S_j \leq 1.05$ from 2007 to 2023 (i.e., sites without a distinct
dominant regime for PN sensitivity), where S_i is the dominant sensitivity, and S_j is the one of the other two sensitivities
different from S_i (e.g., if S_i is S_{NO_x} , then S_j is S_{NH_3} or S_{VOC}), to perform reduced-major-axis linear regression and deduce the
wintertime PN sensitivity regime cutoff (Figure S7) (Dang et al., 2023b). In this work, we chose to derive the regime cutoffs
220 in some years to perform the regression. However, it is important to note that long-term trends in the formation sensitivity are
the same whether using individual year or multi-year regressions (Figure S8). We focused on the NO_x -sensitive and NH_3 -
sensitive regime because MWUS PN had limited sensitivity to VOC emissions during wintertime (Section 3.1). After
diagnosing the PN sensitivity for each pixel for each winter season, we analyzed the changes in PN sensitivity from 2007 to
2023.

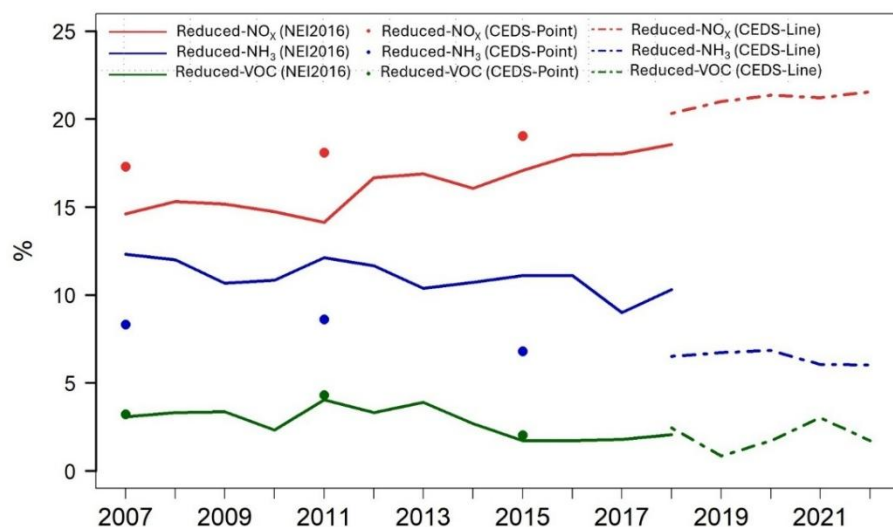
225 **2.5. GEOS-Chem evaluation:**

We perform a series of simulations in GEOS-Chem to assess the sensitivity of PN to changes in precursor gas emissions
from 2007 to 2022. First, we establish the reliability of GEOS-Chem for this analysis by evaluating the ability of the GEOS-
Chem Base simulations to reproduce ground monitoring observations and trends. We compare PN magnitudes and trends
during January and sample GEOS-Chem at the IMPROVE and CSN monitoring locations (Figure S3). On average, GEOS-
230 Chem underestimates wintertime PN mass concentrations by -33.6% compared to ground observations (GEOS-Chem: $1.3 \mu\text{g m}^{-3}$,
 IMPROVE : $1.6 \mu\text{g m}^{-3}$, CSN : $2.3 \mu\text{g m}^{-3}$). The biases in modelled PN may be due to uncertainties in nighttime chemistry,
especially N_2O_5 uptake and the extent to which residual upper-planetary boundary layer PN sinks to the ground, emissions
inventories, aerosol liquid water, and wet deposition of HNO_3 (Norman et al., 2025; Travis et al., 2022; Heald et al., 2012;
Curci et al., 2015; Tang et al., 2021). Despite underestimation, GEOS-Chem shows good agreement with ground monitor
235 trends, indicating that the sensitivity of PN to changes in emissions is captured. PN mass concentrations from GEOS-Chem
show a decreasing trend from 2007 to 2013 ($-10.3 \pm 2.3\% \text{ yr}^{-1}$), which then flattens from 2014 to 2022 ($-0.14 \pm 1.16\% \text{ yr}^{-1}$).
This is consistent with the trends from CSN and IMPROVE on average: PN decreases by $-11.0 \pm 4.5\% \text{ yr}^{-1}$ from 2007 to 2013,
and it flattens afterward to $1.1 \pm 1.9\% \text{ yr}^{-1}$. Thus, GEOS-Chem successfully captures the decrease and subsequent flattening
trends of wintertime PN over both rural (IMPROVE) and urban (CSN) areas from 2007 to 2022. Modeled nitrate wet deposition
240 is overestimated by 139%, but nitrate wet deposition trends are also captured well by GEOS-Chem (Figure S9) (Luo et al.,
2020; Christiansen et al., 2024; Silvern et al., 2019).

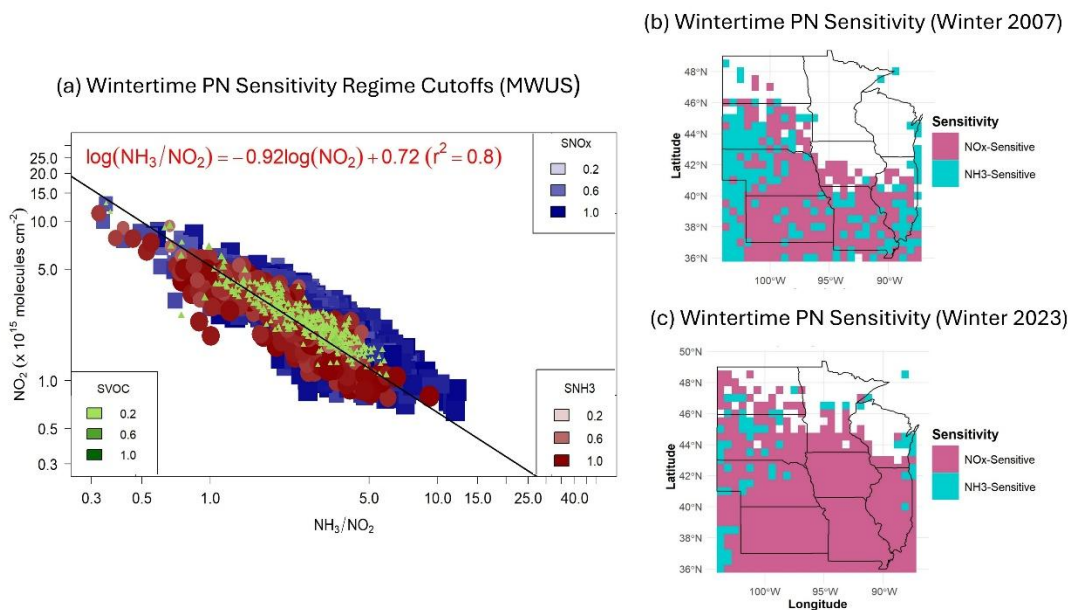
3. Results and Discussions:

3.1. Diagnosing PN sensitivity regime over the MWUS:

MWUS Wintertime : PN Formation Sensitivity from GEOS – Chem (2007 – 2022)



245 Figure 2: The percentage difference in PN mass concentrations between the Base simulations and Reduced-NO_x simulations (red), Base simulations and Reduced-NH₃ simulations (blue), and Base simulations and Reduced-VOC simulations (green). The solid lines indicate sensitivity simulations using the NEI2016 emissions inventory, and the dashed lines and points indicate sensitivity simulations using the CEDS emissions inventory.



250

255

260

Figure 3: Wintertime PN formation sensitivity over the MWUS. Panel (a) shows the wintertime PN diagnostic regime cutoffs using GEOS-Chem and satellite observations. The x-axis is satellite tropospheric NH₃/NO₂ ratio, and the y-axis is satellite NO₂ column densities from OMI. The colors of the data points shown here are GEOS-Chem-calculated local PN sensitivity to each precursor gas (S_i). The data points are GEOS-Chem-calculated sensitivity ratios (S_i/S_j > 1.1) in independent model grid cells. Blue squares represent the NO_x-sensitive regime, red circles represent the NH₃-sensitive regime, and green triangles represent the VOC-sensitive regime. As no pixels are dominated by VOC-sensitive regime (i.e., no S_{voc}/S_j > 1.1.), only pixels with sensitivity values S_{voc} > 0.2 are shown for illustration but not included in calculations. The regression line is derived via reduced-major-axis linear regression using pixels of all years with sensitivity ratios of 0.95 < S_i/S_j < 1.05. Panel (b) and (c) shows the wintertime PN formation sensitivity over the MWUS in 2007 and in 2023, respectively, after satellite grid cell ratios are placed into sensitivity regimes using Equations (4) and (5). In panel (b) and (c), pink indicates NO_x-sensitive regions, and blue indicates NH₃-sensitive regions.

265

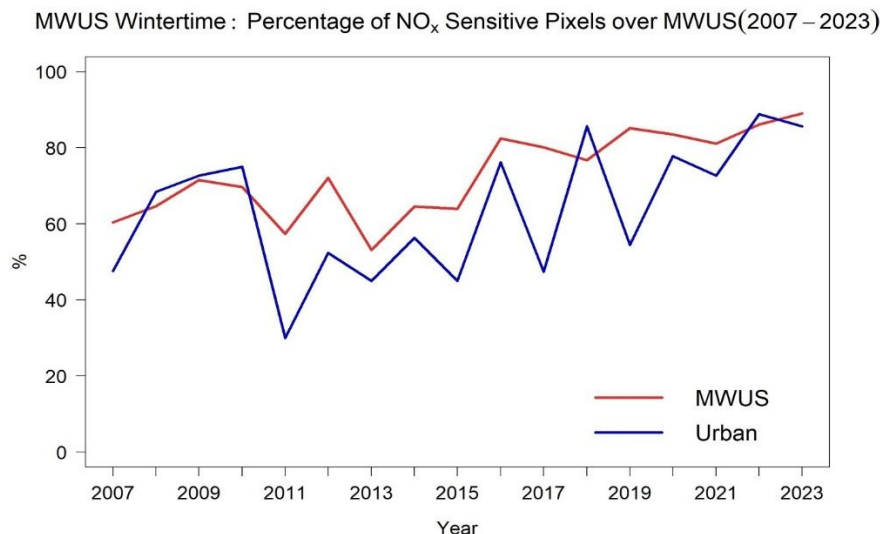
270

The local model sensitivity of PN, S_i, is calculated by Equation (3) for each model grid cell to derive the regime cutoffs using reduced-major-axis linear regression. PN is not sensitive to changes in VOC emissions (Reduced-VOC) at any point during the timeframe. In the Reduced-VOC simulation, changes in PN as a result of a 20% decrease in VOC emissions range from 0.84% to 4.0%, which is substantially lower than changes seen in the Reduced-NO_x and Reduced-NH₃ simulations (range of 6.0% to 21.6%) (Figure 2). Hence, S_{VOC} is excluded from the regression, although it is shown in Figure 3a for illustration.

In Figure 3, each point represents a GEOS-Chem grid cell with a dominant wintertime PN sensitivity regime (i.e., S_i/S_j > 1.1) plotted at its corresponding independent satellite NO₂ column densities and satellite tropospheric NH₃/NO₂ ratios. Some overlap of data points in Figure 3a is expected for two reasons: 1) this figure combines all dominant sites from 2007 to 2022, and 2) wintertime NO_x and NH₃ concentrations shift drastically across the timeframe. As noted previously, the trend in the shift of PN formation regimes is the same regardless of whether we determine formation regimes with individual-year or combined-year data (Figure S8). After performing reduced-major-axis linear regression, the diagnostic cutoffs for NO_x and NH₃-sensitive regimes are expressed by the inequalities (4) and (5).

$$NH_3 - sensitive: \log\left(\frac{NH_3}{NO_2}\right) < 0.72 - 0.92 \times \log(NO_2) \quad (4)$$

$$NO_x - sensitive: \log\left(\frac{NH_3}{NO_2}\right) > 0.72 - 0.92 \times \log(NO_2) \quad (5)$$



275 **Figure 4: The percentage of NO_x-sensitive pixel counts over the MWUS (red) and over just urban areas (blue) (2007 -2023).**

The percent differences in PN mass concentrations between the Base and Reduced-NO_x simulations increase from 14.6% in 2007 to 21.6% in 2022. By contrast, the percent differences between the Base and Reduced-NH₃ simulations decrease from 12.3% in 2007 to 6.0% in 2022 (Figure 2). Together, these results suggest that PN is becoming increasingly sensitive to NO_x emissions and less sensitive to NH₃ emissions. Our satellite-based results are consistent with an independent analysis of chemical mechanics (Text S1) and PN thermodynamic sensitivity (Text S2). This is covered in more detail in the supplemental, but briefly, we use the thermodynamic equilibrium model ISORROPIA-II to investigate the thermodynamic sensitivity of PN and the roles of other potential drivers of trends (Fountoukis and Nenes, 2007). Our results suggest that the thermodynamics of wintertime PN formation over the MWUS is shifting away from NH₃-sensitivity (Figure S10 and Text S2), consistent with our satellite-based diagnostic, and that PN trends cannot be explained by changes in aerosol liquid water, meteorological variability, or N₂O₅ uptake (Text S1).

280
285

Quantitatively, the NO_x-sensitive regime is the dominant regime in the MWUS, as the distribution of NO_x-sensitive grid cells is always > 50% (Figure 4), and this is especially prevalent over the Central MWUS (Movie S1). In 2007, 60.4% of the diagnosed pixels are NO_x-sensitive, but this increases to 89.0% in 2023 (Figures 3 and 4). The largest shift in PN sensitivity over the MWUS occurs after 2013, where 76.9% of the total diagnosed pixels are classified as NO_x-sensitive on average from 2014 to 2023, compared to 66.0% on average from 2007 to 2013 (Figure 4). Satellite NO₂ and NH₃ column uncertainties may propagate to errors in classification. We find that accounting for the extreme ends of the uncertainty may cause a change in

290

diagnosed sensitivity regime in ~30% of the classified grid cells, but wintertime PN formation shows a consistent shift toward a predominant NO_x -sensitive regime after 2013 in all cases (Figure S11). PN sensitivity over urban areas also follows the shifts in regime found for the rural MWUS (Figure 4). Our findings are consistent with previous studies which diagnosed PN sensitivity over agricultural areas. Holt et al. (2015) found that the wintertime sensitivity of inorganic $\text{PM}_{2.5}$ over Northern Midwest has become more sensitive to NO_x emissions in 2012 compared to 2005 (Holt et al., 2015). Wintertime PN formation is also NO_x -sensitive over South Korea, where 76% of anthropogenic NH_3 emissions originate from livestock (Oak et al., 2025). In addition, Guo et al. (2018) found that PN formation is more sensitive to NO_x than NH_3 during wintertime over an agricultural area in the Netherlands (Guo et al., 2018). Overall, our findings suggest that MWUS PN formation was sensitive to both changes in NO_x and NH_3 emissions from 2007 to 2013, but this has shifted to a predominantly NO_x -sensitive regime afterward.

The distribution of PN sensitivity regimes from 2007 to 2023 over the MWUS is shown in Movie S1. Spatially, much of the shift in PN formation sensitivity is driven by changes in emissions over the eastern portion of the MWUS, which is more densely populated. In 2007, MWUS PN formation was highly sensitive to NH_3 emissions over the eastern part of MWUS (Figure 3b,c), which shifted strongly toward NO_x sensitivity by 2023. The shift in formation regime is consistent with the spatial trends of NO_2 and NH_3 column densities (Movie S2 – Movie S4, Figure S12).

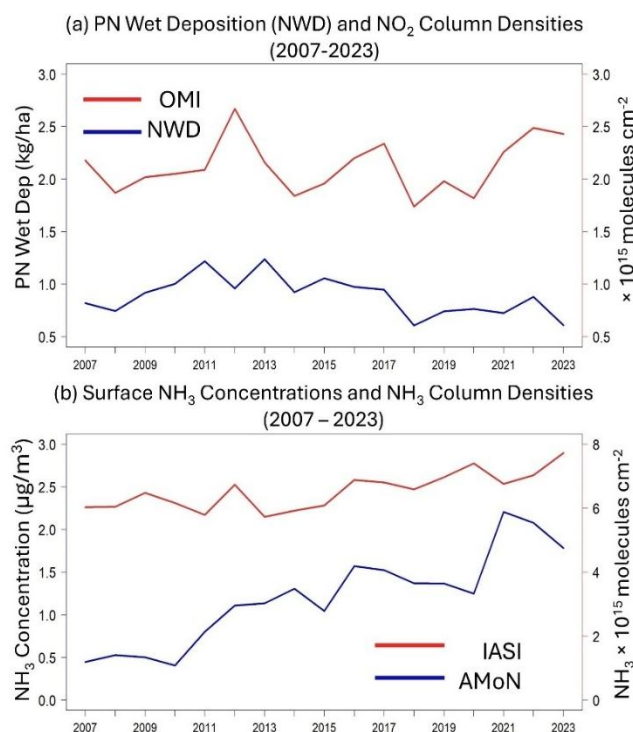
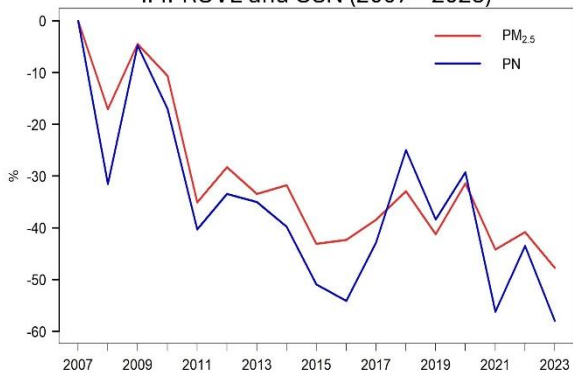


Figure 5: Wintertime NO_2 and NH_3 column density trends over the MWUS (2007 – 2023). Panel (a) shows the trends between nitrate wet deposition (NWD) (blue) from NADP and NO_2 column density over the MWUS (red) from OMI. Panel (b) shows the trends between surface NH_3 concentrations (blue) from AMoN and NH_3 column density (red) from IASI (2007-2023).

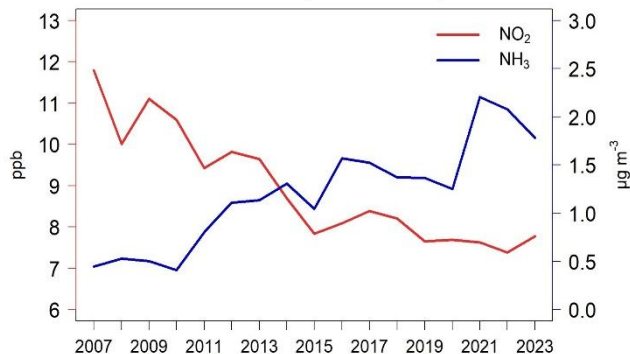
The shift in PN sensitivity regime over the MWUS is consistent with the trends in wintertime NO₂ and NH₃ satellite column densities and ground observations. We find that these trends cannot be explained by meteorological variability, and instead rely on aerosol chemistry and thermodynamic processes (Figure S13 and Text S2). The trends of satellite NO₂ and NH₃ column densities from 2007 to 2023 with uncertainties are shown in Figure S14. Trends in NO₂ column densities stayed relatively flat from 2007 to 2023 ($0.48 \pm 0.60\% \text{ yr}^{-1}$) (Figure 5a). The relatively flat trends in satellite NO₂ are consistent with prior analyses of satellite trends over rural areas and nitrate wet deposition (NWD), a good proxy for regional NO₂. Prior decreases in rural NO₂ have flattened out over time due to the increasing relative importance of static background NO₂ sources, such as soils, lightning, and biomass burning, as anthropogenic NO_x emissions decrease (Figure S4) (Christiansen et al., 2024; Jiang et al., 2018; Silvern et al., 2019). This is consistent with the flattening trends in NWD, a proxy for regional NO_x trends (Figure S15). When we compare satellite NO₂ to EPA monitors over urban areas, which are dominated by anthropogenic NO_x emissions, by matching grid cells exactly, we find that NO₂ concentrations and NO₂ column density exhibit decreasing trends, which are $-2.5 \pm 0.5\% \text{ yr}^{-1}$ and $-1.2 \pm 0.8\% \text{ yr}^{-1}$, respectively. In contrast, wintertime NH₃ column densities have increased from 2007 to 2023 by $1.3 \pm 0.3\% \text{ yr}^{-1}$ (Figure 5b). The increase in NH₃ columns agree with increases in surface NH₃ concentrations reported by AMoN ($8.2 \pm 1.0\% \text{ yr}^{-1}$) (Figure 5b) and prior studies (Wang et al., 2023b). Interestingly, NH₃ column densities significantly increase by $2.2 \pm 0.5\% \text{ yr}^{-1}$ from 2014 to 2023, a stronger rate compared to the relatively flat trends from 2007 to 2013 ($-0.1 \pm 1.2\% \text{ yr}^{-1}$). This acceleration in NH₃ column density over the MWUS may be attributed to wintertime agricultural emissions (Vo and Christiansen, 2024; Wang et al., 2023b; Yu et al., 2018). Over the MWUS, fertilizer application contributes ~62% of total agricultural NH₃ emissions, and livestock waste contributes ~38% in 2020 (US EPA, 2023). The observed trends from both satellites and at the surface are consistent with PN sensitivity shifts toward the NO_x-sensitive regime. This suggests that controlling wintertime NO_x emissions over the MWUS is a critical mitigation strategy for reducing wintertime PN and PM_{2.5} burden.

3.2. Implications for particulate matter:

(a) Wintertime PN and PM_{2.5} Trends over MWUS using IMPROVE and CSN (2007 – 2023)



(b) Wintertime NO₂ and NH₃ Trends over MWUS using EPA and AMoN (2007 – 2023)

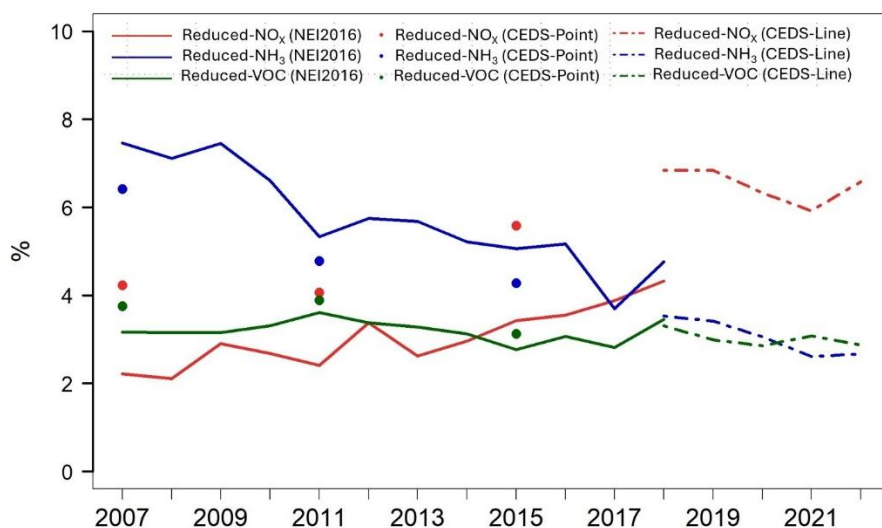


335

Figure 6: Panel (a) shows the relative changes of PM_{2.5} (red) and PN (blue) since 2007 over the MWUS using IMPROVE and CSN ground monitoring observations. Panel (b) shows the wintertime trends in NO₂ (red) and NH₃ (blue) concentrations over the MWUS using AMoN and EPA ground monitoring observations.

340 Throughout the region, PN is the dominant wintertime component of the particle matrix. The average contributions of particle chemical components are 25.7% for PN, 10.3% for SO₄²⁻, and 19.5% for OC over urban areas. The contribution of PN, SO₄²⁻ and OC to total PM_{2.5} mass concentrations over rural areas are 32.3%, 18.7%, and 25.3%, respectively (Figure S16). Trends in observed PM_{2.5} and PN also align with our findings regarding formation sensitivity. Observations from the IMPROVE network and CSN show decreases in wintertime PM_{2.5} mass concentrations of $-3.3 \pm 0.6\% \text{ yr}^{-1}$ from 2007 to 2023
 345 over the MWUS (Figure 6a). Prior to 2013, the decrease in PM_{2.5} was stronger compared to the trends after 2013, during which time the trends in PM_{2.5} started to level off ($-7.1 \pm 1.9\% \text{ yr}^{-1}$ from 2007 to 2013, $-1.0 \pm 1.0\% \text{ yr}^{-1}$ from 2014 to 2023). This similarity persists in PN mass concentrations. Overall, PN shows a decreasing trend of $-3.4 \pm 0.9\% \text{ yr}^{-1}$. Prior to 2013, PN decreases by $-6.3 \pm 2.9\% \text{ yr}^{-1}$, while the decreases after 2013 slow to $-1.0 \pm 2.3\% \text{ yr}^{-1}$. These results suggest that PN and PM_{2.5} trends are mostly driven by changes in NO₂, especially after 2013, when NH₃ concentrations increase strongly and NO₂ remains
 350 relatively constant (Figure 6b). These trends are consistent across urban and rural sites (Figure S13). Our model simulations also suggest that overall PM_{2.5} formation sensitivity is becoming more sensitive to NO_x emissions (Figure 7), similar to our findings for PN (Figure 2).

MWUS Wintertime : PM_{2.5} Formation Sensitivity from GEOS – Chem (2007 – 2022)



355 **Figure 7:** The percentage difference in PM_{2.5} mass concentrations between the Base simulations and Reduced-NO_x simulations (red), Base simulations and Reduced-NH₃ simulations (blue), and Base simulations and Reduced-VOC simulations (green). The solid lines represent sensitivity simulations using the NEI2016 emissions inventory. The dashed lines and points represent sensitivity simulations using the CEDS emissions inventory.

The prominence of PN in the particle matrix, the similarity of PN and PM_{2.5} trends, and the increasing sensitivity of both
360 PN and PM_{2.5} to NO_x emissions all suggest that PN may be critical for determining wintertime PM_{2.5} burden and trends over
the MWUS (Figure S17). Hence, reducing PN would be most effective for reducing PM_{2.5} burden over the MWUS during
winter. The most impactful timeframe for controlling wintertime PM_{2.5} via NH₃ reduction in the MWUS may have already
passed. Prior to the mid-2010s, regulating NH₃ emissions during wintertime would have decreased PM_{2.5} mass concentrations
more effectively over the MWUS compared to reducing NO_x emissions, as reported in many studies starting in the mid-2000s
365 (Gu et al., 2021; Makar et al., 2009; Pinder et al., 2007; Yang et al., 2022). This is consistent with our findings prior to 2010,
in which the changes in PM_{2.5} burden are more sensitive to changes in NH₃ emissions in almost half the region. However,
during this time period, regulations focused on NO_x and SO₂ emissions, increasing formation sensitivity to NO_x as emissions
continued to decrease. After the late 2000s, reducing NH₃ emissions has become increasingly less effective in controlling
wintertime PN and thus PM_{2.5} burden. The percentage difference in wintertime PM_{2.5} mass concentrations between the Base
and Reduced-NO_x simulations gradually increases by 0.31% yr⁻¹ from 2007 to 2022 (2.2% in 2007, 6.6% in 2022), while it
370 decreases by -0.33% yr⁻¹ in the Reduced-NH₃ simulation (7.5% in 2007, 2.7% in 2022). This is consistent with the shifts in
wintertime PN sensitivity. These trends are captured using both NEI2016 and CEDS emissions inventories (Figure 7). Our
findings are also consistent with more recent studies. In 2015, it was estimated that effective mitigation of PM_{2.5} in the MWUS
may require anthropogenic NH₃ emissions cuts of 60–90%. (Guo et al., 2024). This requirement will have only become harder
375 to achieve since then. Similarly, Pan et al. (2024) suggested that regulating NH₃ is becoming less effective as secondary
inorganic aerosols have become less sensitive to NH₄⁺, and reductions in NH₄⁺ concentrations of 40–70% would be needed to
reduce annual secondary inorganic aerosols over the rural United States (Pan et al., 2024). Holt et al. (2015) found that the
sensitivity of wintertime inorganic PM_{2.5} shifted toward NO_x emissions from 2005 to 2012, especially over the northern
Midwest (Holt et al., 2015). Currently and in the future, NO_x emissions reductions are likely the most effective way to control
380 wintertime PN formation and PM_{2.5} burden in the MWUS.

It should be noted that, while PN is most sensitive to NO_x in the winter, reducing NH₃ emissions can still decrease PM_{2.5}
burden with significant benefits within this season. Over the MWUS, despite having the lowest agricultural NH₃ emissions
compared to other seasons, a reduction of 0.01 Tg NH₃ could decrease PM_{2.5} burden up to 3.7% during wintertime, suggesting
that reducing agricultural NH₃ emissions may still have significant impacts over agricultural regions (Vo and Christiansen,
385 2024). Controlling NO_x emissions will become increasingly costly, but agricultural NH₃ emissions may be able to be targeted
at a lower cost (Gu et al., 2021; Makar et al., 2009; Muller and Mendelsohn, 2007; Pinder et al., 2007). In addition, controlling
local NO_x production may become less effective for mitigating air quality concerns as regional sources (e.g., lightning, soils)
become dominant contributors to NO_x emissions and trends. Careful consideration of technological advancements and
economic concerns will be needed for new regulations aimed at reducing PM_{2.5} burden over agricultural regions. This study
390 was only focused on wintertime PN and PM_{2.5} burden, and sensitivity conditions in other seasons may differ, as both NO_x and
NH₃ emissions show distinct seasonal patterns. This is an area for future investigation.

4. Conclusion:

Our study shows that wintertime PN formation is becoming more sensitive to NO_x emissions over the MWUS from 2007 to 2023. This is consistent with the relatively flat trends in satellite NO₂ column densities ($0.48 \pm 0.60\% \text{ yr}^{-1}$) and the continuous increases in satellite NH₃ column densities ($1.3 \pm 0.3\% \text{ yr}^{-1}$) from 2007 to 2023 over MWUS. VOCs do not influence the formation of PN over the MWUS. Our results indicate that it is most chemically effective to control NO_x emissions to reduce wintertime PN and PM_{2.5} burden. The MWUS might have missed the most impactful window to control wintertime PM_{2.5} by reducing NH₃ emissions. Future work to diagnose PN formation sensitivity over the MWUS across other seasons is needed to understand whether controlling NO_x emissions is effective year-round. This work provides a chemical perspective for policymakers interested in effective emissions controls to improve air quality and human health over agriculturally intensive regions.

Code, data, or code and data availability

Data and R code used in this publication are available at <https://doi.org/10.5281/zenodo.18021326>.

Supplement link

The link to the supplement will be included by Copernicus, if applicable.

Author contributions

AC designed and directed the projects. TV performed the research, compiled and analyzed the data, conducted model simulations, and prepared the manuscript.

Competing interests

The authors declare that they have no conflict of interest.

Disclaimer

Copernicus Publications remains neutral with regard to jurisdictional claims made in the text, published maps, institutional affiliations, or any other geographical representation in this paper. While Copernicus Publications makes every effort to include appropriate place names, the final responsibility lies with the authors. Views expressed in the text are those of the authors and do not necessarily reflect the views of the publisher.

Acknowledgements

We would like to acknowledge Krotkov et al. (2019) for publicly available NO₂ column densities and Clarisse et al. (2018a, 2018b) for NH₃ column densities. The computational for this work was performed on the high-performance computing infrastructure operated by Research Support Solutions in the Division of IT at the University of Missouri, Columbia MO on the Hellbender cluster (DOI: <https://doi.org/10.32469/10355/97710>). We thank the National Atmospheric Deposition Program for providing open-access data for gaseous NH₃ concentrations and nitrate wet deposition over the United States. We also acknowledge the United States Environmental Agency for publicly available surface NO₂ concentrations, PM_{2.5} mass concentrations and particle chemical speciation data over urban areas. We also acknowledge the Interagency Monitoring of PROtected Visual Environments (IMRPOVE) for the public availability of PM_{2.5} mass concentrations and particle chemical speciation data over rural areas. Lastly, we thank Daniel Jacob for the development and public availability of GEOS-Chem.

Review statement

The review statement will be added by Copernicus Publications listing the handling editor as well as all contributing referees according to their status anonymous or identified.

References

- 2016v1 Platform: <https://www.epa.gov/air-emissions-modeling/2016v1-platform>, last access: 31 October 2025.
- Ammonia Monitoring Network: <https://nadp.slh.wisc.edu/networks/ammonia-monitoring-network/>, National Atmospheric Deposition Program [data set], last accessed 2025-11-01.
- Boersma, K. F., Vinken, G. C. M., and Eskes, H. J.: Representativeness errors in comparing chemistry transport and chemistry climate models with satellite UV–Vis tropospheric column retrievals, *Geoscientific Model Development*, 9, 875–898, <https://doi.org/10.5194/gmd-9-875-2016>, 2016.
- Cao, Y., Ma, Q., Chu, B., and He, H.: Homogeneous and heterogeneous photolysis of nitrate in the atmosphere: state of the science, current research needs, and future prospects, *Frontiers of Environmental Science & Engineering*, 17, 1–18, <https://doi.org/10.1007/s11783-023-1648-6>, 2022.
- Christiansen, A., Mickley, L. J., and Hu, L.: Constraining long-term NO_x emissions over the United States and Europe using nitrate wet deposition monitoring networks, *Atmospheric Chemistry and Physics*, 24, 4569–4589, <https://doi.org/10.5194/acp-24-4569-2024>, 2024.
- Christiansen, A. E., Carlton, A. G., and Porter, W. C.: Changing Nature of Organic Carbon over the United States, *Environ. Sci. Technol.*, 54, 10524–10532, <https://doi.org/10.1021/acs.est.0c02225>, 2020.
- Clarisse, L. and Coheur, P.-F. (2018). Reanalyzed daily IASI/Metop-A ULB-LATMOS ammonia (NH₃) L2 product (total column) [data set]. Aeris. <https://doi.org/10.25326/12>, last accessed 2025-05.

- Clarisse, L. and Coheur, P.-F. (2018). Reanalyzed daily IASI/Metop-B ULB-LATMOS ammonia (NH₃) L2 product (total column) [data set]. Aeris. <https://doi.org/10.25326/13>, last accessed 2025-05.
- 450 Clerbaux, C., Boynard, A., Clarisse, L., George, M., Hadji-Lazaro, J., Herbin, H., Hurtmans, D., Pommier, M., Razavi, A., Turquety, S., Wespes, C., and Coheur, P.-F.: Monitoring of atmospheric composition using the thermal infrared IASI/MetOp sounder, *Atmospheric Chemistry and Physics*, 9, 6041–6054, <https://doi.org/10.5194/acp-9-6041-2009>, 2009.
- 455 Dang, R., Jacob, D. J., Shah, V., Eastham, S. D., Fritz, T. M., Mickley, L. J., Liu, T., Wang, Y., and Wang, J.: Background nitrogen dioxide (NO₂) over the United States and its implications for satellite observations and trends: effects of nitrate photolysis, aircraft, and open fires, *Atmospheric Chemistry and Physics*, 23, 6271–6284, <https://doi.org/10.5194/acp-23-6271-2023>, 2023a.
- Dang, R., Jacob, D. J., Zhai, S., Coheur, P., Clarisse, L., Van Damme, M., Pendergrass, D. C., Choi, J., Park, J., Liu, Z., and Liao, H.: Diagnosing the Sensitivity of Particulate Nitrate to Precursor Emissions Using Satellite Observations of Ammonia and Nitrogen Dioxide, *Geophysical Research Letters*, 50, e2023GL105761, <https://doi.org/10.1029/2023GL105761>, 2023b.
- 460 Dang, R., Jacob, D. J., Zhai, S., Yang, L. H., Pendergrass, D. C., Coheur, P., Clarisse, L., Van Damme, M., Choi, J., Park, J., Liu, Z., Xie, P., and Liao, H.: A Satellite-Based Indicator for Diagnosing Particulate Nitrate Sensitivity to Precursor Emissions: Application to East Asia, Europe, and North America, *Environ. Sci. Technol.*, 58, 20101–20113, <https://doi.org/10.1021/acs.est.4c08082>, 2024.
- 465 Demerjian, K. L.: A review of national monitoring networks in North America, *Atmospheric Environment*, 34, 1861–1884, [https://doi.org/10.1016/S1352-2310\(99\)00452-5](https://doi.org/10.1016/S1352-2310(99)00452-5), 2000.
- Di, Q., Wang, Y., Zanobetti, A., Wang, Y., Koutrakis, P., Choirat, C., Dominici, F., and Schwartz, J. D.: Air Pollution and Mortality in the Medicare Population, *New England Journal of Medicine*, 376, 2513–2522, <https://doi.org/10.1056/NEJMoa1702747>, 2017.
- 470 Fenn, M. E., Bytnerowicz, A., Schilling, S. L., Vallano, D. M., Zavaleta, E. S., Weiss, S. B., Morozumi, C., Geiser, L. H., and Hanks, K.: On-road emissions of ammonia: An underappreciated source of atmospheric nitrogen deposition, *Science of The Total Environment*, 625, 909–919, <https://doi.org/10.1016/j.scitotenv.2017.12.313>, 2018.
- Fioletov, V., McLinden, C. A., Griffin, D., Krotkov, N., Liu, F., and Eskes, H.: Quantifying urban, industrial, and background changes in NO₂ during the COVID-19 lockdown period based on TROPOMI satellite observations, *Atmospheric Chemistry and Physics*, 22, 4201–4236, <https://doi.org/10.5194/acp-22-4201-2022>, 2022.
- 475 Fountoukis, C. and Nenes, A.: ISORROPIA II: a computationally efficient thermodynamic equilibrium model for K⁺; Ca²⁺; Mg²⁺; NH₄⁺; Na⁺; SO₄²⁻; NO₃⁻; Cl⁻; H₂O aerosols, *Atmospheric Chemistry and Physics*, 7, 4639–4659, <https://doi.org/10.5194/acp-7-4639-2007>, 2007.
- 480 Franchin, A., Fibiger, D. L., Goldberger, L., McDuffie, E. E., Moravek, A., Womack, C. C., Crosman, E. T., Docherty, K. S., Dube, W. P., Hoch, S. W., Lee, B. H., Long, R., Murphy, J. G., Thornton, J. A., Brown, S. S., Baasandorj, M., and Middlebrook, A. M.: Airborne and ground-based observations of ammonium-nitrate-dominated aerosols in a shallow boundary layer during intense winter pollution episodes in northern Utah, *Atmospheric Chemistry and Physics*, 18, 17259–17276, <https://doi.org/10.5194/acp-18-17259-2018>, 2018.
- 485 Gelaro, R., McCarty, W., Suárez, M. J., Todling, R., Molod, A., Takacs, L., Randles, C. A., Darmenov, A., Bosilovich, M. G., Reichle, R., Wargan, K., Coy, L., Cullather, R., Draper, C., Akella, S., Buchard, V., Conaty, A., Silva, A. M. da, Gu, W., Kim, G.-K., Koster, R., Lucchesi, R., Merkova, D., Nielsen, J. E., Partyka, G., Pawson, S., Putman, W., Rienecker, M., Schubert, S.

- D., Sienkiewicz, M., and Zhao, B.: The Modern-Era Retrospective Analysis for Research and Applications, Version 2 (MERRA-2), *Journal of Climate*, 30, 5419–5454, <https://doi.org/10.1175/JCLI-D-16-0758.1>, 2017.
- Gen, M., Liang, Z., Zhang, R., Go, B. R., and Chan, C. K.: Particulate nitrate photolysis in the atmosphere, *Environ. Sci.: Atmos.*, 2, 111–127, <https://doi.org/10.1039/D1EA00087J>, 2022.
- 490 Gu, B., Zhang, L., Van Dingenen, R., Vieno, M., Van Grinsven, H. J., Zhang, X., Zhang, S., Chen, Y., Wang, S., Ren, C., Rao, S., Holland, M., Winiwarter, W., Chen, D., Xu, J., and Sutton, M. A.: Abating ammonia is more cost-effective than nitrogen oxides for mitigating PM_{2.5} air pollution, *Science*, 374, 758–762, <https://doi.org/10.1126/science.abf8623>, 2021.
- Guenther, A. B., Jiang, X., Heald, C. L., Sakulyanontvittaya, T., Duhl, T., Emmons, L. K., and Wang, X.: The Model of Emissions of Gases and Aerosols from Nature version 2.1 (MEGAN2.1): an extended and updated framework for modeling
495 biogenic emissions, *Geoscientific Model Development*, 5, 1471–1492, <https://doi.org/10.5194/gmd-5-1471-2012>, 2012.
- Guo, H., Otjes, R., Schlag, P., Kiendler-Scharr, A., Nenes, A., and Weber, R. J.: Effectiveness of ammonia reduction on control of fine particle nitrate, *Atmospheric Chemistry and Physics*, 18, 12241–12256, <https://doi.org/10.5194/acp-18-12241-2018>, 2018.
- Guo, Y., Zhang, L., Winiwarter, W., Grinsven, H. J. M. van, Wang, X., Li, K., Pan, D., Liu, Z., and Gu, B.: Ambitious nitrogen abatement is required to mitigate future global PM_{2.5} air pollution toward the World Health Organization targets, *One Earth*,
500 7, 1600–1613, <https://doi.org/10.1016/j.oneear.2024.08.007>, 2024.
- Hand, J. L., Schichtel, B. A., Pitchford, M., Malm, W. C., and Frank, N. H.: Seasonal composition of remote and urban fine particulate matter in the United States, *Journal of Geophysical Research: Atmospheres*, 117, <https://doi.org/10.1029/2011JD017122>, 2012.
- 505 He, T.-L., Jones, D. B. A., Miyazaki, K., Huang, B., Liu, Y., Jiang, Z., White, E. C., Worden, H. M., and Worden, J. R.: Deep Learning to Evaluate US NO_x Emissions Using Surface Ozone Predictions, *Journal of Geophysical Research: Atmospheres*, 127, e2021JD035597, <https://doi.org/10.1029/2021JD035597>, 2022.
- Hoesly, R. M., Smith, S. J., Feng, L., Klimont, Z., Janssens-Maenhout, G., Pitkanen, T., Seibert, J. J., Vu, L., Andres, R. J., Bolt, R. M., Bond, T. C., Dawidowski, L., Kholod, N., Kurokawa, J., Li, M., Liu, L., Lu, Z., Moura, M. C. P., O'Rourke, P.
510 R., and Zhang, Q.: Historical (1750–2014) anthropogenic emissions of reactive gases and aerosols from the Community Emissions Data System (CEDS), *Geoscientific Model Development*, 11, 369–408, <https://doi.org/10.5194/gmd-11-369-2018>, 2018.
- Holt, J., Selin, N. E., and Solomon, S.: Changes in Inorganic Fine Particulate Matter Sensitivities to Precursors Due to Large-Scale US Emissions Reductions, *Environ. Sci. Technol.*, 49, 4834–4841, <https://doi.org/10.1021/acs.est.5b00008>, 2015.
- 515 Hu, L., Millet, D. B., Baasandorj, M., Griffis, T. J., Turner, P., Helmig, D., Curtis, A. J., and Hueber, J.: Isoprene emissions and impacts over an ecological transition region in the U.S. Upper Midwest inferred from tall tower measurements, *Journal of Geophysical Research: Atmospheres*, 120, 3553–3571, <https://doi.org/10.1002/2014JD022732>, 2015.
- Hudman, R. C., Moore, N. E., Mebust, A. K., Martin, R. V., Russell, A. R., Valin, L. C., and Cohen, R. C.: Steps towards a mechanistic model of global soil nitric oxide emissions: implementation and space based-constraints, *Atmospheric Chemistry and Physics*, 12, 7779–7795, <https://doi.org/10.5194/acp-12-7779-2012>, 2012.
- 520 Interagency Monitoring of PROtected Visual Environments. <https://views.cira.colostate.edu/fed/QueryWizard/>. (accessed 2025-11-01) [Dataset].

- Inventory Collaborative 2016v1 Emissions Modeling Platform.
 525 https://views.cira.colostate.edu/wiki/Attachments/Inventory%20Collaborative/Documentation/2016v1/after_comments/National-Emissions-Collaborative_2016v1_nonpoint-ag_25Feb2020.pdf. (accessed March 12, 2026)
- Jefferson, A., Hageman, D., Morrow, H., Mei, F., and Watson, T.: Seven years of aerosol scattering hygroscopic growth measurements from SGP: Factors influencing water uptake, *Journal of Geophysical Research: Atmospheres*, 122, 9451–9466,
 530 <https://doi.org/10.1002/2017JD026804>, 2017.
- Jiang, Z., McDonald, B. C., Worden, H., Worden, J. R., Miyazaki, K., Qu, Z., Henze, D. K., Jones, D. B. A., Arellano, A. F., Fischer, E. V., Zhu, L., and Boersma, K. F.: Unexpected slowdown of US pollutant emission reduction in the past decade, *Proceedings of the National Academy of Sciences*, 115, 5099–5104, <https://doi.org/10.1073/pnas.1801191115>, 2018.
- Keller, C. A., Long, M. S., Yantosca, R. M., Da Silva, A. M., Pawson, S., and Jacob, D. J.: HEMCO v1.0: a versatile, ESMF-compliant component for calculating emissions in atmospheric models, *Geoscientific Model Development*, 7, 1409–1417,
 535 <https://doi.org/10.5194/gmd-7-1409-2014>, 2014.
- Koster, R. D., Darnenov, A. S., and da Silva, A. M.: The Quick Fire Emissions Dataset (QFED): Documentation of Versions 2.1, 2.2 and 2.4: Technical Report Series on Global Modeling and Data Assimilation - Volume 38, 2015.
- Krotkov, N. A.; Lamsal, L. N.; Marchenko, S. V.; Bucsela, E. J.; Swartz, W. H.; Joiner, J.; the OMI Core Team (2019). OMI/Aura Nitrogen Dioxide (NO₂) Total and Tropospheric Column 1-orbit L2 Swath 13x24 km V003, Greenbelt, MD, USA, Goddard Earth Sciences Data and Information Services Center (GES DISC) [data set]. DOI: 10.5067/Aura/OMI/DATA2017, last accessed 2025-05.
 540
- Lamb, D. and Bowersox, V.: The national atmospheric deposition program: an overview, *Atmospheric Environment*, 34, 1661–
 545 1663, [https://doi.org/10.1016/S1352-2310\(99\)00425-2](https://doi.org/10.1016/S1352-2310(99)00425-2), 2000.
- Lamsal, L. N., Martin, R. V., van Donkelaar, A., Celarier, E. A., Bucsela, E. J., Boersma, K. F., Dirksen, R., Luo, C., and Wang, Y.: Indirect validation of tropospheric nitrogen dioxide retrieved from the OMI satellite instrument: Insight into the seasonal variation of nitrogen oxides at northern midlatitudes, *Journal of Geophysical Research: Atmospheres*, 115, <https://doi.org/10.1029/2009JD013351>, 2010.
- Lamsal, L. N., Krotkov, N. A., Vasilkov, A., Marchenko, S., Qin, W., Yang, E.-S., Fasnacht, Z., Joiner, J., Choi, S., Haffner, D., Swartz, W. H., Fisher, B., and Bucsela, E.: Ozone Monitoring Instrument (OMI) Aura nitrogen dioxide standard product version 4.0 with improved surface and cloud treatments, *Atmospheric Measurement Techniques*, 14, 455–479, <https://doi.org/10.5194/amt-14-455-2021>, 2021.
 550
- Luo, G., Yu, F., and Moch, J. M.: Further improvement of wet process treatments in GEOS-Chem v12.6.0: impact on global distributions of aerosols and aerosol precursors, *Geoscientific Model Development*, 13, 2879–2903, <https://doi.org/10.5194/gmd-13-2879-2020>, 2020.
 555
- Makar, P. A., Moran, M. D., Zheng, Q., Cousineau, S., Sassi, M., Duhamel, A., Besner, M., Davignon, D., Crevier, L.-P., and Bouchet, V. S.: Modelling the impacts of ammonia emissions reductions on North American air quality, *Atmospheric Chemistry and Physics*, 9, 7183–7212, <https://doi.org/10.5194/acp-9-7183-2009>, 2009.
- Malm, W. C., Sisler, J. F., Huffman, D., Eldred, R. A., and Cahill, T. A.: Spatial and seasonal trends in particle concentration and optical extinction in the United States, *Journal of Geophysical Research: Atmospheres*, 99, 1347–1370, <https://doi.org/10.1029/93JD02916>, 1994.
 560

- Muller, N. Z. and Mendelsohn, R.: Measuring the damages of air pollution in the United States, *Journal of Environmental Economics and Management*, 54, 1–14, <https://doi.org/10.1016/j.jeem.2006.12.002>, 2007.
- 565 National Trends Network. <https://nadp.slh.wisc.edu/networks/national-trends-network/> (accessed 2025-11-01) [Dataset].
- Nenes, A., Pandis, S. N., Weber, R. J., and Russell, A.: Aerosol pH and liquid water content determine when particulate matter is sensitive to ammonia and nitrate availability, *Atmospheric Chemistry and Physics*, 20, 3249–3258, <https://doi.org/10.5194/acp-20-3249-2020>, 2020.
- 570 Oak, Y. J., Jacob, D. J., Pendergrass, D. C., Dang, R., Colombi, N. K., Chong, H., Lee, S., Kuk, S. K., and Kim, J.: Air quality trends and regimes in South Korea inferred from 2015–2023 surface and satellite observations, *Atmospheric Chemistry and Physics*, 25, 3233–3252, <https://doi.org/10.5194/acp-25-3233-2025>, 2025.
- 575 Palmer, P. I., Jacob, D. J., Chance, K., Martin, R. V., Spurr, R. J. D., Kurosu, T. P., Bey, I., Yantosca, R., Fiore, A., and Li, Q.: Air mass factor formulation for spectroscopic measurements from satellites: Application to formaldehyde retrievals from the Global Ozone Monitoring Experiment, *Journal of Geophysical Research: Atmospheres*, 106, 14539–14550, <https://doi.org/10.1029/2000JD900772>, 2001.
- Pan, D., Mauzerall, D. L., Wang, R., Guo, X., Puchalski, M., Guo, Y., Song, S., Tong, D., Sullivan, A. P., Schichtel, B. A., Collett, J. L., and Zondlo, M. A.: Regime shift in secondary inorganic aerosol formation and nitrogen deposition in the rural United States, *Nat. Geosci.*, 17, 617–623, <https://doi.org/10.1038/s41561-024-01455-9>, 2024.
- 580 Paulot, F., Jacob, D. J., Pinder, R. W., Bash, J. O., Travis, K., and Henze, D. K.: Ammonia emissions in the United States, European Union, and China derived by high-resolution inversion of ammonium wet deposition data: Interpretation with a new agricultural emissions inventory (MASAGE_NH3), *JGR Atmospheres*, 119, 4343–4364, <https://doi.org/10.1002/2013JD021130>, 2014.
- 585 Paulot, F., Ginoux, P., Cooke, W. F., Donner, L. J., Fan, S., Lin, M.-Y., Mao, J., Naik, V., and Horowitz, L. W.: Sensitivity of nitrate aerosols to ammonia emissions and to nitrate chemistry: implications for present and future nitrate optical depth, *Atmospheric Chemistry and Physics*, 16, 1459–1477, <https://doi.org/10.5194/acp-16-1459-2016>, 2016.
- Petetin, H., Sciare, J., Bressi, M., Gros, V., Rosso, A., Sanchez, O., Sarda-Estève, R., Petit, J.-E., and Beekmann, M.: Assessing the ammonium nitrate formation regime in the Paris megacity and its representation in the CHIMERE model, *Atmospheric Chemistry and Physics*, 16, 10419–10440, <https://doi.org/10.5194/acp-16-10419-2016>, 2016.
- 590 Pinder, R. W., Adams, P. J., and Pandis, S. N.: Ammonia Emission Controls as a Cost-Effective Strategy for Reducing Atmospheric Particulate Matter in the Eastern United States, *Environ. Sci. Technol.*, 41, 380–386, <https://doi.org/10.1021/es060379a>, 2007.
- Pitchford, M. L., Poirot, Richard L., Schichtel, Bret A., and Malm, W. C.: Characterization of the Winter Midwestern Particulate Nitrate Bulge, *Journal of the Air & Waste Management Association*, 59, 1061–1069, <https://doi.org/10.3155/1047-3289.59.9.1061>, 2009.
- 595 Pokharel, A., Hennessy, D. A., and Wu, F.: Health burden associated with tillage-related PM2.5 pollution in the United States, and mitigation strategies, *Science of The Total Environment*, 903, 166161, <https://doi.org/10.1016/j.scitotenv.2023.166161>, 2023.
- 600 Puchalski, M. A., Rogers, C. M., Baumgardner, R., Mishoe, K. P., Price, G., Smith, M. J., Watkins, N., and Lehmann, C. M.: A statistical comparison of active and passive ammonia measurements collected at Clean Air Status and Trends Network (CASTNET) sites, *Environ. Sci.: Processes Impacts*, 17, 358–369, <https://doi.org/10.1039/C4EM00531G>, 2015.

- Qin, C., Fu, X., Wang, T., Gao, J., and Wang, J.: Control of fine particulate nitrate during severe winter haze in “2+26” cities, *Journal of Environmental Sciences*, 136, 261–269, <https://doi.org/10.1016/j.jes.2022.12.016>, 2024.
- Romer Present, P. S., Zare, A., and Cohen, R. C.: The changing role of organic nitrates in the removal and transport of NO_x, *Atmospheric Chemistry and Physics*, 20, 267–279, <https://doi.org/10.5194/acp-20-267-2020>, 2020.
- 605 Sarwar, G., Hogrefe, C., Henderson, B. H., Mathur, R., Gilliam, R., Callaghan, A. B., Lee, J., and Carpenter, L. J.: Impact of particulate nitrate photolysis on air quality over the Northern Hemisphere, *Science of The Total Environment*, 917, 170406, <https://doi.org/10.1016/j.scitotenv.2024.170406>, 2024.
- Shah, V., Jacob, D. J., Dang, R., Lamsal, L. N., Strode, S. A., Steenrod, S. D., Boersma, K. F., Eastham, S. D., Fritz, T. M., Thompson, C., Peischl, J., Bourgeois, I., Pollack, I. B., Nault, B. A., Cohen, R. C., Campuzano-Jost, P., Jimenez, J. L.,
610 Andersen, S. T., Carpenter, L. J., Sherwen, T., and Evans, M. J.: Nitrogen oxides in the free troposphere: implications for tropospheric oxidants and the interpretation of satellite NO₂ measurements, *Atmospheric Chemistry and Physics*, 23, 1227–1257, <https://doi.org/10.5194/acp-23-1227-2023>, 2023.
- Shi, L., Rosenberg, A., Wang, Y., Liu, P., Danesh Yazdi, M., Réquia, W., Steenland, K., Chang, H., Sarnat, J. A., Wang, W., Zhang, K., Zhao, J., and Schwartz, J.: Low-Concentration Air Pollution and Mortality in American Older Adults: A National Cohort Analysis (2001–2017), *Environ. Sci. Technol.*, 56, 7194–7202, <https://doi.org/10.1021/acs.est.1c03653>, 2022.
615
- Shimadera, H., Hayami, H., Chatani, S., Morino, Y., Mori, Y., Morikawa, T., Yamaji, K., and Ohara, T.: Sensitivity analyses of factors influencing CMAQ performance for fine particulate nitrate, *Journal of the Air & Waste Management Association*, 64, 374–387, <https://doi.org/10.1080/10962247.2013.778919>, 2014.
- Silvern, R. F., Jacob, D. J., Mickley, L. J., Sulprizio, M. P., Travis, K. R., Marais, E. A., Cohen, R. C., Laughner, J. L., Choi, S., Joiner, J., and Lamsal, L. N.: Using satellite observations of tropospheric NO₂ columns to infer long-term trends in US NO_x emissions: the importance of accounting for the free tropospheric NO₂ background, *Atmospheric Chemistry and Physics*, 19, 8863–8878, <https://doi.org/10.5194/acp-19-8863-2019>, 2019.
620
- Simone, N. W., Stettler, M. E. J., and Barrett, S. R. H.: Rapid estimation of global civil aviation emissions with uncertainty quantification, *Transportation Research Part D: Transport and Environment*, 25, 33–41, <https://doi.org/10.1016/j.trd.2013.07.001>, 2013.
625
- Solomon, P. A., Crumpler, D., Flanagan, J. B., Jayanty, R. K. M., Rickman, E. E., and McDade, C. E.: U.S. National PM_{2.5} Chemical Speciation Monitoring Networks—CSN and IMPROVE: Description of networks, *Journal of the Air & Waste Management Association*, 64, 1410–1438, <https://doi.org/10.1080/10962247.2014.956904>, 2014.
- Sun, K., Tao, L., Miller, D. J., Pan, D., Golston, L. M., Zondlo, M. A., Griffin, R. J., Wallace, H. W., Leong, Y. J., Yang, M. M., Zhang, Y., Mauzerall, D. L., and Zhu, T.: Vehicle Emissions as an Important Urban Ammonia Source in the United States and China, *Environ. Sci. Technol.*, 51, 2472–2481, <https://doi.org/10.1021/acs.est.6b02805>, 2017.
630
- Tang, G., Wang, Y., Liu, Y., Wu, S., Huang, X., Yang, Y., Wang, Y., Ma, J., Bao, X., Liu, Z., Ji, D., Li, T., Li, X., Wang, Y.: Low particulate nitrate in the residual layer in autumn over the North China Plain, *Science of the Total Environment*, 782, 146845, <https://doi.org/10.1016/j.scitotenv.2021.146845>, 2021.
- 635 Tessum, C. W., Apte, J. S., Goodkind, A. L., Muller, N. Z., Mullins, K. A., Paoletta, D. A., Polasky, S., Springer, N. P., Thakrar, S. K., Marshall, J. D., and Hill, J. D.: Inequity in consumption of goods and services adds to racial–ethnic disparities in air pollution exposure, *Proceedings of the National Academy of Sciences*, 116, 6001–6006, <https://doi.org/10.1073/pnas.1818859116>, 2019.

- 640 Tong, D. Q., Lamsal, L., Pan, L., Ding, C., Kim, H., Lee, P., Chai, T., Pickering, K. E., and Stajner, I.: Long-term NO_x trends over large cities in the United States during the great recession: Comparison of satellite retrievals, ground observations, and emission inventories, *Atmospheric Environment*, 107, 70–84, <https://doi.org/10.1016/j.atmosenv.2015.01.035>, 2015.
- United States Environmental Protection Agency (US EPA). 2020 NEI Supporting Data and Summaries. <https://www.epa.gov/air-emissions-inventories/2020-nei-supporting-data-and-summaries>. Last updated on March 30, 2023 (accessed on April 1, 2026).
- 645 United States Environmental Protection Agency (US EPA). AirData website File Download page, https://aqs.epa.gov/aqsweb/airdata/download_files.html#Daily (accessed 2025-11-01) [Dataset].
- 650 United States Environmental Protection Agency. Ammonia Emissions: What to Know before You Regulate Official White Paper of USDA Agricultural Air Quality Task Force 2014. <https://www.nrcs.usda.gov/sites/default/files/2022-10/AAQTF-AccomplishmentsAmmonia-White-Paper.pdf>. (accessed 2025-10-31).
- Van Damme, M., Clarisse, L., Heald, C. L., Hurtmans, D., Ngadi, Y., Clerbaux, C., Dolman, A. J., Erisman, J. W., and Coheur, P. F.: Global distributions, time series and error characterization of atmospheric ammonia (NH₃) from IASI satellite observations, *Atmospheric Chemistry and Physics*, 14, 2905–2922, <https://doi.org/10.5194/acp-14-2905-2014>, 2014.
- 655 Van Damme, M., Whitburn, S., Clarisse, L., Clerbaux, C., Hurtmans, D., and Coheur, P.-F.: Version 2 of the IASI NH₃ neural network retrieval algorithm: near-real-time and reanalysed datasets, *Atmospheric Measurement Techniques*, 10, 4905–4914, <https://doi.org/10.5194/amt-10-4905-2017>, 2017.
- 660 Van Damme, M., Clarisse, L., Franco, B., Sutton, M. A., Erisman, J. W., Wichink Kruit, R., van Zanten, M., Whitburn, S., Hadji-Lazaro, J., Hurtmans, D., Clerbaux, C., and Coheur, P.-F.: Global, regional and national trends of atmospheric ammonia derived from a decadal (2008–2018) satellite record, *Environ. Res. Lett.*, 16, 055017, <https://doi.org/10.1088/1748-9326/abd5e0>, 2021.
- Visser, A. J., Boersma, K. F., Ganzeveld, L. N., and Krol, M. C.: European NO_x emissions in WRF-Chem derived from OMI: impacts on summertime surface ozone, *Atmospheric Chemistry and Physics*, 19, 11821–11841, <https://doi.org/10.5194/acp-19-11821-2019>, 2019.
- 665 Vo, T. and Christiansen, A. E.: Impact of Recent Agricultural Ammonia Increases on Fine Particulate Matter Burden over the Midwestern United States, *ACS Earth Space Chem.*, 8, 2209–2217, <https://doi.org/10.1021/acsearthspacechem.4c00180>, 2024.
- 670 Walters, W. W., Karod, M., Willcocks, E., Baek, B. H., Blum, D. E., and Hastings, M. G.: Quantifying the importance of vehicle ammonia emissions in an urban area of northeastern USA utilizing nitrogen isotopes, *Atmospheric Chemistry and Physics*, 22, 13431–13448, <https://doi.org/10.5194/acp-22-13431-2022>, 2022.
- Wang, H., Lu, K., Tan, Z., Chen, X., Liu, Y., and Zhang, Y.: Formation mechanism and control strategy for particulate nitrate in China, *Journal of Environmental Sciences*, 123, 476–486, <https://doi.org/10.1016/j.jes.2022.09.019>, 2023a.
- 675 Wang, H., Liu, X., Wu, C., and Lin, G.: Regional to global distributions, trends, and drivers of biogenic volatile organic compound emission from 2001 to 2020, *Atmospheric Chemistry and Physics*, 24, 3309–3328, <https://doi.org/10.5194/acp-24-3309-2024>, 2024.
- Wang, R., Pan, D., Guo, X., Sun, K., Clarisse, L., Van Damme, M., Coheur, P.-F., Clerbaux, C., Puchalski, M., and Zondlo, M. A.: Bridging the spatial gaps of the Ammonia Monitoring Network using satellite ammonia measurements, *Atmospheric Chemistry and Physics*, 23, 13217–13234, <https://doi.org/10.5194/acp-23-13217-2023>, 2023b.

- 680 Wang, Y., Ge, C., Castro Garcia, L., Jenerette, G. D., Oikawa, P. Y., and Wang, J.: Improved modelling of soil NO_x emissions in a high temperature agricultural region: role of background emissions on NO₂ trend over the US, *Environ. Res. Lett.*, 16, 084061, <https://doi.org/10.1088/1748-9326/ac16a3>, 2021.
- Wang, Y. X., McElroy, M. B., Jacob, D. J., and Yantosca, R. M.: A nested grid formulation for chemical transport over Asia: Applications to CO, *Journal of Geophysical Research: Atmospheres*, 109, <https://doi.org/10.1029/2004JD005237>, 2004.
- 685 Wang, Z., Jing, B., Shi, X., Tong, S., Wang, W., and Ge, M.: Importance of water-soluble organic acid on the hygroscopicity of nitrate, *Atmospheric Environment*, 190, 65–73, <https://doi.org/10.1016/j.atmosenv.2018.07.010>, 2018.
- Warner, J. X., Dickerson, R. R., Wei, Z., Strow, L. L., Wang, Y., and Liang, Q.: Increased atmospheric ammonia over the world's major agricultural areas detected from space, *Geophysical Research Letters*, 44, 2875–2884, <https://doi.org/10.1002/2016GL072305>, 2017.
- 690 Wen, L., Xue, L., Wang, X., Xu, C., Chen, T., Yang, L., Wang, T., Zhang, Q., and Wang, W.: Summertime fine particulate nitrate pollution in the North China Plain: increasing trends, formation mechanisms and implications for control policy, *Atmospheric Chemistry and Physics*, 18, 11261–11275, <https://doi.org/10.5194/acp-18-11261-2018>, 2018.
- Wiegand, R., Battye, W. H., Myers, C. B., and Aneja, V. P.: Particulate Matter and Ammonia Pollution in the Animal Agricultural-Producing Regions of North Carolina: Integrated Ground-Based Measurements and Satellite Analysis, *Atmosphere*, 13, 821, <https://doi.org/10.3390/atmos13050821>, 2022.
- 695 Womack, C. C., McDuffie, E. E., Edwards, P. M., Bares, R., de Gouw, J. A., Docherty, K. S., Dubé, W. P., Fibiger, D. L., Franchin, A., Gilman, J. B., Goldberger, L., Lee, B. H., Lin, J. C., Long, R., Middlebrook, A. M., Millet, D. B., Moravek, A., Murphy, J. G., Quinn, P. K., Riedel, T. P., Roberts, J. M., Thornton, J. A., Valin, L. C., Veres, P. R., Whitehill, A. R., Wild, R. J., Warneke, C., Yuan, B., Baasandorj, M., and Brown, S. S.: An Odd Oxygen Framework for Wintertime Ammonium Nitrate Aerosol Pollution in Urban Areas: NO_x and VOC Control as Mitigation Strategies, *Geophysical Research Letters*, 46, 4971–4979, <https://doi.org/10.1029/2019GL082028>, 2019.
- 700 Wu, L., Li, X., and Ro, C.-U.: Hygroscopic Behavior of Ammonium Sulfate, Ammonium Nitrate, and their Mixture Particles, *Asian Journal of Atmospheric Environment*, 13, 196–211, <https://doi.org/10.5572/ajae.2019.13.3.196>, 2019.
- Wu, W., Jin, Y., and Carlsten, C.: Inflammatory health effects of indoor and outdoor particulate matter, *Journal of Allergy and Clinical Immunology*, 141, 833–844, <https://doi.org/10.1016/j.jaci.2017.12.981>, 2018.
- 705 Xiong, Y., Du, K., and Huang, Y.: One-third of global population at cancer risk due to elevated volatile organic compounds levels, *npj Clim Atmos Sci*, 7, 54, <https://doi.org/10.1038/s41612-024-00598-1>, 2024.
- Xu, Z., Liu, M., Zhang, M., Song, Y., Wang, S., Zhang, L., Xu, T., Wang, T., Yan, C., Zhou, T., Sun, Y., Pan, Y., Hu, M., Zheng, M., and Zhu, T.: High efficiency of livestock ammonia emission controls in alleviating particulate nitrate during a severe winter haze episode in northern China, *Atmospheric Chemistry and Physics*, 19, 5605–5613, <https://doi.org/10.5194/acp-19-5605-2019>, 2019.
- 710 Yang, Y., Liu, L., Bai, Z., Xu, W., Zhang, F., Zhang, X., Liu, X., and Xie, Y.: Comprehensive quantification of global cropland ammonia emissions and potential abatement, *Science of The Total Environment*, 812, 151450, <https://doi.org/10.1016/j.scitotenv.2021.151450>, 2022.
- 715 Yang, Y., Liu, L., Liu, P., Ding, J., Xu, H., and Liu, S.: Improved global agricultural crop- and animal-specific ammonia emissions during 1961–2018, *Agriculture, Ecosystems & Environment*, 344, 108289, <https://doi.org/10.1016/j.agee.2022.108289>, 2023.

Yu, F., Nair, A. A., and Luo, G.: Long-Term Trend of Gaseous Ammonia Over the United States: Modeling and Comparison With Observations, *Journal of Geophysical Research: Atmospheres*, 123, 8315–8325, <https://doi.org/10.1029/2018JD028412>, 2018.

720 Zhai, S., Jacob, D. J., Wang, X., Liu, Z., Wen, T., Shah, V., Li, K., Moch, J. M., Bates, K. H., Song, S., Shen, L., Zhang, Y., Luo, G., Yu, F., Sun, Y., Wang, L., Qi, M., Tao, J., Gui, K., Xu, H., Zhang, Q., Zhao, T., Wang, Y., Lee, H. C., Choi, H., and Liao, H.: Control of particulate nitrate air pollution in China, *Nat. Geosci.*, 14, 389–395, <https://doi.org/10.1038/s41561-021-00726-z>, 2021.

725 Zhai, S., Jacob, D. J., Pendergrass, D. C., Colombi, N. K., Shah, V., Yang, L. H., Zhang, Q., Wang, S., Kim, H., Sun, Y., Choi, J.-S., Park, J.-S., Luo, G., Yu, F., Woo, J.-H., Kim, Y., Dibb, J. E., Lee, T., Han, J.-S., Anderson, B. E., Li, K., and Liao, H.: Coarse particulate matter air quality in East Asia: implications for fine particulate nitrate, *Atmospheric Chemistry and Physics*, 23, 4271–4281, <https://doi.org/10.5194/acp-23-4271-2023>, 2023.